Optimization of a marine cycloidal propeller using experimental blade-controlled platform

Guillaume Fasse, Matthieu Sacher, Frederic Hauville, Gregory Germain

Optimization of a marine cycloidal propeller using experimental blade-controlled platform

G. FASSE[a,1], M. SACHER[b], F. HAUVILLE[a], G. GERMAIN[c]

a. Naval Academy Research Institute (IRENav), BCRM Brest, CC600, 29240 Brest Cedex 9, France
b. ENSTA Bretagne, CNRS UMR 6027, IRDL, 2 rue Francois Verny, 29806 Brest Cedex9, France
c. Ifremer, Hydrodynamic & Metocean Service F-62200 Boulogne-sur-Mer, France
1. Mail: guillaume.fasse@ecole-navale.fr

Abstract :

In recent years, innovative naval propulsion systems have been investigated thanks to the growing development of unmanned underwater vehicles. Cycloidal propellers are promising alternative concepts to the usual screw propellers. As bio-inspired technology, these systems use mechanical energy from unsteady hydrodynamic forces generated by blades oscillation like natural marine animal swimmers.
As an academic platform, the French Naval Academy Research Institute developed a large-scale experimental cycloidal propeller with the aim of running diverse pitch motions to evaluate performances of cross-flow propellers. Blades' pitching is here performed by servo-motors in order to control each blade independently. While common cycloidal propellers use mechanical blade actuators which restrain the blade motion possibilities, this blade-controlled platform allows new investigations of interesting research area in marine propulsion.
The platform is widely instrumented with load and torque sensors to measure instantaneous hydrodynamic forces during the rotation of the blades. Experiments, performed at the Ifremer current flume tank, first reveal that for classical sinusoidal pitch laws, performances are depending on the operating point (advance parameter λ) : the higher the advance parameter, the lower the sinusoidal amplitude must be for a better efficiency. These results are detailed in a previous paper written by Fasse et al. These results confirm the requirement of an adaptable pitch control for cycloidal propeller to boost their performances regarding the operation mode.
Thus this paper deals with an experimental optimization, based on surrogates models (Efficient Global Optimization). This optimization is undertaken to surpass the performance of the propeller with parameterized pitch laws. This parameterization consists on modeling the pitch law by a spline defined through relevant control points corresponding to the optimization parameters. This method authorizes a wide range of possible motion taking account of the platform speed limits. Multi-objective optimization is performed for total thrust and efficiency maximizing. Results show that a trade-off is necessary between thrust and efficiency. Finally, Pareto Front is determined to get the best compromise of thrust and efficiency of the propeller.

Keywords: Cycloidal propulsion, Experimental optimization, Multi-objective surrogate-based optimization

1 Introduction

Cycloidal propellers are characterized by the rotation of several blades around an axis perpendicular to the advance direction (opposed to conventional propellers for which the rotation axis is generally aligned with the advance direction). This first rotation is called main rotation, given by the rotational speed Ω and related to the azimuth angle θ ($\Omega = d\theta/dt$). Each blade is also rotating around their own axis during the main rotation of the whole system (like helicopter's blades). This secondary rotation is mainly called pitch rotation, related to the blade pitch angle β or ϕ (depending of the definition of the angle). This particular motion creates strong unsteady hydrodynamic forces which produces lift and drag during the main rotation. The combination of the two rotations reproduces the motion of natural marine swimmers, especially studied by Triantafyllou et al [1]. For propulsive purpose, the part of hydrodynamic force in the direction of the ship advance produces the thrust force F_X whereas the part in the perpendicular direction is called side force F_Y. These propellers can easily orientate the thrust over 360° by shifting the blade pitch law over the main rotation angle.

For this type of propulsion, two kinematic modes are commonly defined according to the advance parameter λ which is the ratio of the ship advance speed V_a and the blade peripheral speed $V_r = \Omega R$, R is the propeller radius:

$$\lambda = \frac{V_a}{V_r} \tag{1}$$

Epicycloidal mode is defined for λ<1 (Figure 1). For this mode, rotational speed is higher than advance speed. This mode produces a high thrust and strong manoeuvrability for low advance speed (limited by the maximal main rotation speed). On the other hand, trochoidal mode defined for λ>1 (Figure 2), is used to reach higher advance speed but with a lack of efficiency during starting phases (not adapted when V_a is near zero). The blade motion is completely different between these two modes. Indeed for epicyloidal mode, the blade chord is roughly following the tangent of the main rotation (because ΩR is higher than V_a), whereas for trochoidal mode the blade oscillates around the advance direction.

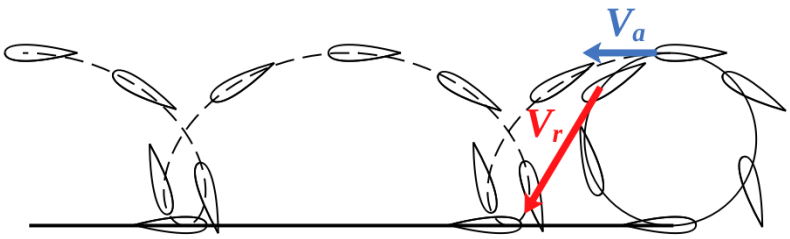

Figure 1: Epicycloidal path of a blade

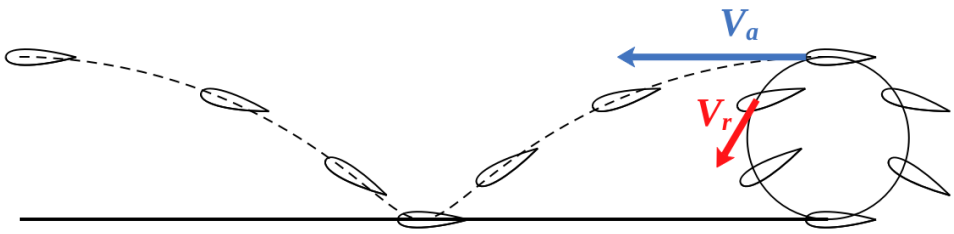

Figure 2: Trochoidal path of a blade

As an interesting marine propulsion system, cycloidal propeller have been studied by the IRENav with

the developpment of an blade-controlled plateform [2]. Thanks to an electrical blade-command design, this platform allows to reproduce blades' kinematic from all conceivable movements (trochoidal or epicycloidal kinematics). This electrical blade-command also allows authors to perform pitch law optimization to improve performances of current cycloidal propellers. The aim of this article is to present an experimental optimization using a Gaussian process based method, coded by Sacher [4], to maximize both thrust and efficiency of cycloidal propellers. The optimization uses experimental measurements collected from the instrumented blade-controlled patform. Experiments are performed at the Ifremer current tank. These experimental facilities are described in the first section as well as the parameterization of the pitch laws. The second section deals with the optimization method overview. Finally results of sinusoidal laws are summarized and compared to the results of the optimization for λ=1.2 simultaneously from thrust and efficiency aspects.

2 Optimization problem

2.1 Context

Cross-flow propeller, also called cycloidal propeller, generates a vectorial thrust which can be adapted in norm and direction. The main control parameter of this type of propulsion is the way the blades are moving through the incoming flow which is called pitch law. Indeed, cycloidal propeller uses lift forces generated by the blades through the flow during the whole rotation. So the pitch law is essential to the design and the performance of a cycloidal propeller, therefore it is the purpose of the optimization presented in this paper.

Most of existing cross-flow technologies use a mechanical system to operate the blade pitch motion as is the case for the renowned Voith-Schneider Propeller [5] for which blades are actuated by a rod/crank mechanism. More recently Roesler [3] designed an experimental platform with a system of crankshaft and concentric collars to generate trochoidal motions and they performed measurements at the UNH testing facility in USA. Mechanical system implies a symmetrical blade pitch law to ensure the stability and the load balancing of the propeller. This is also the simplest way to design a mechanical cycloidal propeller. But because of the complexity of the flow and the high perturbed wake, the blade behaviour has no reason to be symmetrical between up and downstream flow. Indeed during the upstream half-rotation, the flow viewed by the blades is calm and undisturbed, whereas in the downstream half-rotation the blades encounter the wake of upstream other blades regularly agitated by vortex or free surface suction phenomenon.

To deal with this challenge, authors choose to go through an experimental optimization of the cycloidal propeller pitch law using a non-symmetrical parameterization and an experimental platform able to run this kind of law.

2.2 Blade-controlled platform

To perform the optimization, the experimental blade controlled cross-flow propeller, called SHIVA developed by the authors, is operating at the Ifremer wave and current flume tank. Figure 3 gives an overview of the platform and its positioning at the flume tank.

SHIVA is composed of a triangular frame [F] in which three blades [I] are mounted. These blades are rotating thanks to three servo-motors [E] that gives them independent motions.

The outer frame [D] allows the platform to be elevated above the tank in order to dive just the blades

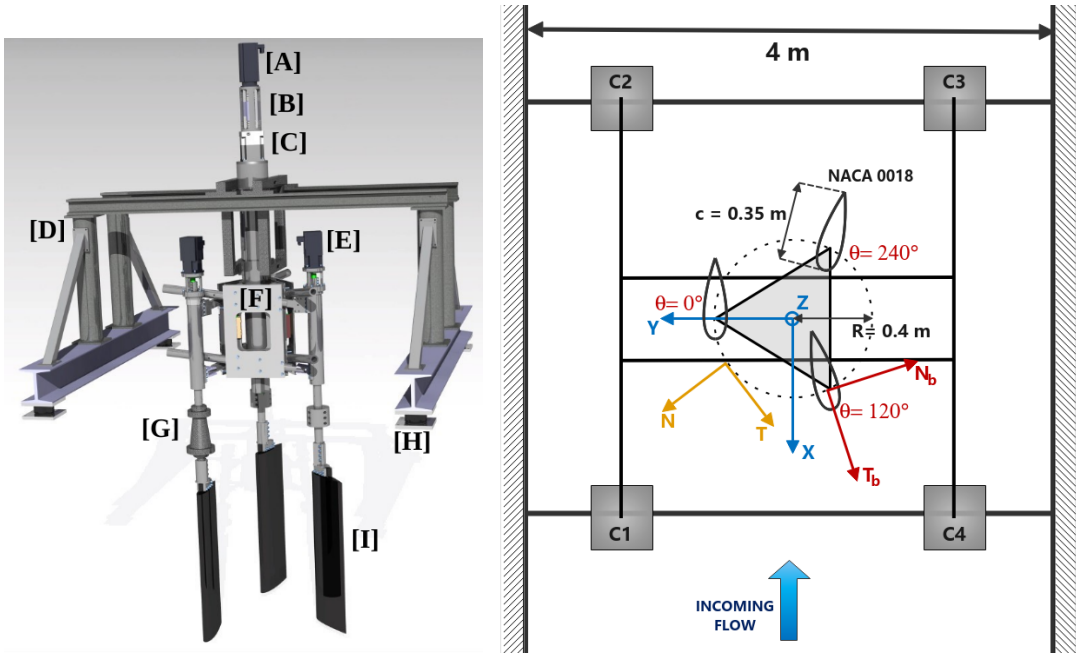

Figure 3: Blade-controlled platform and its positioning at the current flume tank

under the water line.

The design of the platform allows users to change the rotor diameter from 0.4 m to 0.8 m. The blade number N is fixed at 3. Each blade has a chord length c = 0.35 m and a span l = 1 m with a blade cross section of NACA 0018. For the presented measurements the diameter is fixed at D = 0.8 m. These dimensions lead to a solidity of the propeller σ = 2.62 ($\sigma = \frac{2Nc}{D}$).

The particularity of this experimental platform lies on the electric blade pitch command. The triangular frame is driven by the 2.5kW main motor [A] located at the top of the platform. A 50-ratio speed reducer [C] is used to increase the torque and fit the rotational speed for our experiment values (∼0-50 RPM). Each blade is independently actuated by a 0.8kW auxiliary motor [E]. The blades rotate around the quarter of their chord, close to the aerodynamic center for the NACA 0018.

This rotation is called blade pitch and is referred to as the oriented angle φ between the tank flow direction (X-axis) and the blade chord. The pitch angle can also be defined as the oriented angle β between the ortho-radial line of the main rotation and the blade chord (see Figure 4). These two pitch angles are linked by the relation $\theta = \varphi - \beta$. The azimuth position of a blade θ is the position of its chord quarter on the main rotation disk, and for an arbitrary time Δt, θ=$\Omega\Delta t$ where Ω is the main rotational speed.

Expression of the pitch angle in function of the azimuth position is the pitch law. These laws are tabulated as discrete functions on an embedded micro-controller unit which send regulation orders directly to the speed controllers for each blades in order to follow the reference pitch law. These laws are loaded on the platform via Ethernet liaison from a computer located alongside the tank. Pitch laws can be loaded even during the rotation which helps to gain precious time during optimization procedure.

Because the pitch motion is electric and no more mechanical, a delay of the real blade position can occur when the motors can't follow the reference pitch according to their limits in speed and torque. Figures 5 gives the pitch tracking for two laws: a sinusoidal law at the left and an epicycloidal law at the right. These pitch tracking measurements have been performed during in water experiments with a tank speed V=0.8 m/s and a rotational speed Ω set for the desired λ value (Ω=8.68 RPM corresponding to λ=2.2 and Ω=21.2 RPM corresponding to λ=0.9). The pitch law for trochoidal mode is given by the φ angle (pitch

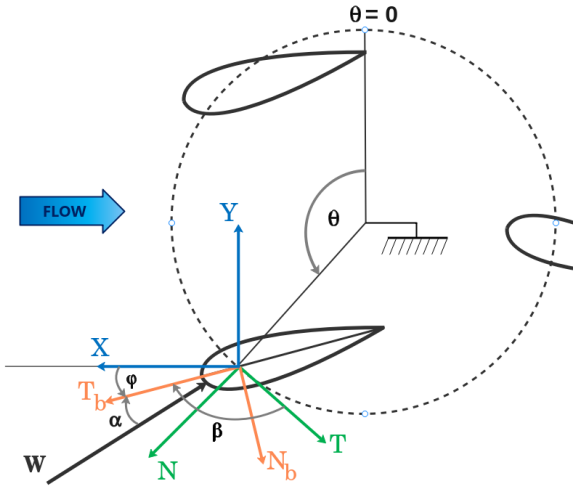

Figure 4: Representation of angles for an arbitrary position θ and an arbitrary relative velocity W

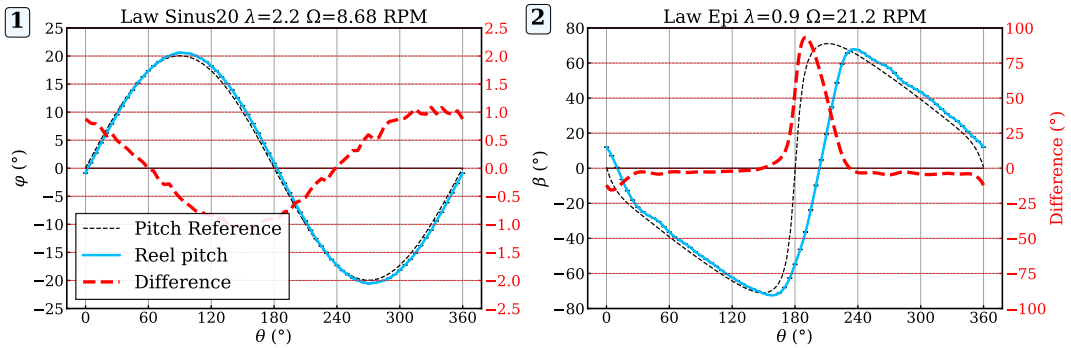

Figure 5: Pitch tracking for two different laws: 1) 20-Sinusoidal law in trochoidal mode (λ=2.2, V=0.8 m/s, Ω=8.68 RPM) and 2) Epicycloidal law (λ=0.9, V=0.8 m/s, Ω=21.2 RPM). Left axis refers to pitch angle in degrees(φ for trocho mode and β for epi mode) whereas right axis refers to the difference in degrees between real and reference pitch.

around the inlet flow direction) whereas the pitch is expressed by β angle in epicycloidal mode (pitch around the tangent of the main rotation). The left axis (in red) of each sub-figure gives the difference between the reference and the real pitch. These results show that for trochoidal mode a maximal error of 1° occurs when the gradient ($d\varphi/d\theta$) is highest. For epicycloidal mode, there is a blade reversal at θ=180°, which characterizes epicycloid motions. This quick motion is not well following by the motors because of the speed limits (the error reaches almost 100°). After this huge error, the blade keeps a delay which is never caught. A detailed study of the pitch tracking error is given by Fasse in [2].
These limitations in speed involve the use of a law's classification during the optimization procedure (See section 2.3). Indeed, if the pitch tracking error is too high, the pitch law is classified "non-doable". Moreover, with current motorization only trochoidal laws are performed on the platform SHIVA during experiments.

In addition, SHIVA is widely instrumented to measure time-dependant hydrodynamic loads and blade angular positions. Rotary incremental encoders provide angular position of each blade with a precision of 0.088°. They are used simultaneously for the control loop as feedback and for loads measurements as projection angle. The azimuth position is also recorded by a rotary incremental encoders with a precision of 0.014°.
One blade is instrumented with an embedded 5-components load-cell [G] which measure local hydro-

dynamic loads in the direction of the blade's chord $\mathbf{T_b}$ (measuring range of 200 N) and normal to the blade $\mathbf{N_b}$ (measuring range of 900 N). This load-cell also measures the torque $\mathbf{C_b}$ applied on the blade by hydrodynamic loads (measuring range of 60 Nm).
Four fixed 3-components load-cell [H] located between the outer frame I-beams and the tank I-beams provide global solicitations of the propeller in the X,Y and Z directions (measuring range of 5000 N in the X and Y direction and 7000 N for the Z direction). At least, a torque sensor [B] is installed between the main motor and the speed reducer and measures the torque applied on the main driveshaft $\mathbf{C_{tot}}$ (measuring range of 20 Nm).
Due to the wider measuring range of these fixed load-cell, in comparison with the embedded load-cell, post-processing of the loads is done with local hydrodynamic loads (for more precision, refer to [2]). The embedded load-cell measures temporal voltages which are highly disturbed by high frequencies of electromagnetic environment mainly due to the Pulse Width Modulation of speed controllers. Low-pass filter (50Hz cut-frequency) is thus applied on temporal signals. Then voltages are converted into loads thanks to the transfer matrix determined by calibration. Finally, thanks to the acquisition of angular positions, forces in blade reference frame ($\mathbf{F_{N_b}}$, $\mathbf{F_{T_b}}$) are projected into rotor reference frame ($\mathbf{F_N}$, $\mathbf{F_T}$) and absolute reference frame ($\mathbf{F_X}$, $\mathbf{F_Y}$) by equations (2) and (3).

$$\begin{pmatrix} F_T \\ F_N \end{pmatrix} = \begin{pmatrix} \cos(\beta) & -\sin(\beta) \\ -\sin(\beta) & -\cos(\beta) \end{pmatrix} \begin{pmatrix} F_{T_b} \\ F_{N_b} \end{pmatrix} \tag{2}$$

$$\begin{pmatrix} F_X \\ F_Y \end{pmatrix} = \begin{pmatrix} \cos(\theta) & \sin(\theta) \\ -\sin(\theta) & \cos(\theta) \end{pmatrix} \begin{pmatrix} F_T \\ F_N \end{pmatrix} \tag{3}$$

Then instantaneous forces are phase-averaged over at least 30 revolutions to one period, shifted of $\frac{\pi}{3}$ and $\frac{2\pi}{3}$, and summed to give the total force acting on the three blades. Lastly, total thrust coefficient, torque coefficient and hydrodynamic efficiency are calculated as the non-dimensional averaged values:

$$C_{F_X} = \frac{\overline{F_{X_{tot}}}}{0.5\rho S V^2} \qquad C_T = \frac{\overline{C_{tot}}}{0.5\rho S D V^2} \qquad \eta = \frac{\overline{F_{X_{tot}}}\, V}{\overline{C_{tot}}\, \Omega} \tag{4}$$

Where $\overline{F_{X_{tot}}}$ and $\overline{C_{tot}}$ are respectively the mean of total thrust and total torque (measured on the main torque sensor) over 360°, S is the swept frontal area ($S = Dl$) and V the flume tank flow velocity.
These experimental performances are measured and spent through the optimization code to evaluate the objective function. To perform the optimization, the choice of the parameters have to be suited for maximizing the performance of cycloidal propeller. The blade motion is directly linked to the hydrodynamic force generation. And because SHIVA is designed to run all type of blade pitch motion, the parameterization consists in configure the pitch laws with several parameters.

2.3 Parametric model

To proceed the optimization procedure, the first step is to develop an accurate parameterization. Indeed, Efficient Global Optimization methods, used here, allows to decrease the number of optimization step in comparison with genetic methods. But more the number of parameters is high and more the number of optimization step is required.
The method presented in this paper consists in defining the pitch law by a spline passing through four control points which are given by 3 parameters (inspired from Abbaszadeh [6]). Figure 6 illustrates the parameterization for two random laws.

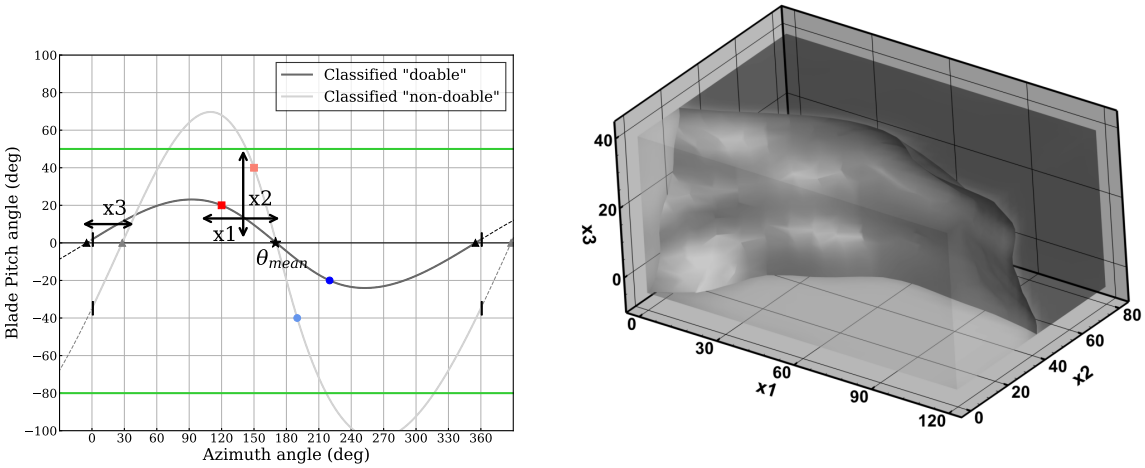

Figure 6: At the left, pitch law parameterization method. At the right, classification iso-surface of "doable" pitch law in the parametric space.

The four control points are the first black triangle, the red square, the blue circle and the last black triangle. These points are defined with three parameters:

1. The first parameter $\mathbf{x_1}$ gives the abscissa of the two central points (red square and blue circle in the Figure 6) by setting the distance of this abscissa and the central position θ_{mean}:

$$x_{red\ square} = \theta_{mean} - \mathbf{x_1}$$
$$x_{blue\ circle} = \theta_{mean} + \mathbf{x_1}$$

2. The second parameter $\mathbf{x_2}$ give the ordinate of these two central points:

$$y_{red\ square} = \mathbf{x_2} \quad ; \quad y_{blue\ circle} = -\mathbf{x_2}$$

3. The third parameter $\mathbf{x_3}$ allows an offset of the law for the zero crossing at the beginning and the end of the spline (the last black triangle is the 2π-offset of the first one).

$$x_{black\ triangle} = \mathbf{x_3} \quad ; \quad y_{black\ triangle} = 0$$

For the presented results, the central position θ_{mean} is set at 170 degrees. This position involves a non-symmetrical pitch law which is the intent of this optimization as explained in the context. The non-symmetrical construction of the law also implies a different gradient between the start (θ=0°) and the end of the spline (θ=360°). To fix this problem, the spline is defined on 10 periods (5 before and 5 after) to ensure the continuity at θ=0° and θ=360° (with an error of 10^{-7}).
Each parameter can move through the following ranges:

- $\Delta x_1 = [0.5 : 120]$
- $\Delta x_2 = [0.5 : 80]$
- $\Delta x_3 = [-5 : 40]$

This method of parameterization implies a weakness which occurs when two points of the spline are to close, the amplitude of the spline can be very high. To avoid this, a classification is used and taking into account during the optimization procedure (detailed in Section 3.2). This classification consists on defining two limits (high and low) to the spline and classify the parameterized spline "doable" if all the points of the spline are between these two limits. These limits are represented in green on the left of the Figure 6 and fixed at $\varphi = 50°$ and $\varphi = -80°$ for the present experiments. These limits have been chosen after experiments considerations: high amplitude laws imply an acceleration for auxiliary motor which is to high (refers to Section 2.2) and in the half downstream it has been sensed that the pitch must be higher than the upstream to give the ability of the blade to "cut" the wake.
For hundred arbitrary laws have been generated over the range of the 3 parameters to estimate the classification model. The right sub-figure of Figure 6 represents this classification model with the iso-surface of 50%-probability of the law to be "doable". This figure shows in the front the area of laws which are considered "doable" and in the back those which have high probability to be "non-doable". During the optimization process, the classification is taking into account and so the area of interest for the new optimized point is always located inside the front area of 50%-probability to be "doable" (see Section 3.2). In addition, if a new optimized law presents a pitch error too high, it is classified "non-doable" and the classification model is updated.

3 Multi-objective Surrogate-based Optimisation

We consider abstract optimization problems, where several objectives have to be minimized simultaneously over a design variable $\Omega \subset \mathbb{R}^d$:

$$\min_{\boldsymbol{x}\in\Omega} f_1(\boldsymbol{x}), \ldots, f_m(\boldsymbol{x}) \quad \text{s.t.} \quad \boldsymbol{g}(\boldsymbol{x}) \leq 0 \tag{5}$$

where $\boldsymbol{x} = (x_i)_{1\leq i\leq d}$ is a vector of design variables, $\boldsymbol{f} = (f_j)_{1\leq j\leq m}$ is a vector of objective functions to be minimized $(f_i : \Omega \mapsto \mathbb{R})$, and $\boldsymbol{g} = (g_k)_{1\leq k\leq p}$ is a vector of inequality constraints $(g_k : \Omega \mapsto \mathbb{R})$. The existence of an optimal solution, minimizing all objectives at once is usually not granted. This leads to the search for an optimal set of solutions, called the Pareto front.

In the present work, individual evaluations of the objective functions are assumed to be very expensive (experiments results). A common approach is then to use surrogate models in place of $\boldsymbol{f}$ to reduce the computational burden related to the evaluations of $\boldsymbol{f}$ [7]. Gaussian processes (GP) [9] are presently considered, which, owing to their statistical nature, provide for each objective function, both a prediction value and a measure of the uncertainty (variance) in this prediction. These features are appealing in the optimization context, as they can be exploited to derive rigorous optimization strategies, by evaluating sequentially the computer models at design vectors that maximize a so-called merit function [10].

In mono-objective problems, GP-based approaches are globally referred to as Efficient Global Optimization (EGO) [11], where the merit function is based on an Expected Improvement (EI) criterion, expressing a trade-off between sampling in promising regions and exploring in unsampled regions. EGO has been successfully applied to complex optimization problems, such as non-linear fluid-structure interaction problems [12, 13] or RANS computations [14].

Over the last few years, surrogate-based approaches have also been proposed to address the multi-objective problem. Indeed, several GP-based multi-objective optimization strategies propose to extend the EI infilling criterion of Jones [11]. The definition of the improvement can then be considered over

the Pareto front, using for instance, Maxi-min distance [15], Euclidean distance [16], or the well-known Hypervolume infilling criterion [17]. In the present work, the latter criterion is used to solve the blade pitch law optimization problem.

In Section 3.1, we summarize the construction of a GP model for an objective function f_j. Definitions of multi-objective surrogate-based merit functions, that are used in the present optimization under non-doable observations, are then provided in Section 3.2.

3.1 GP surrogate construction

In the present Section 3.1, the GP surrogate construction of an objective function f_j is provided. The method is exactly the same for the GP surrogate construction of an inequality constraint function g_k.

We consider a set of n training points $\mathcal{X} = (\boldsymbol{x}_1, \dots, \boldsymbol{x}_n)$, each in Ω. The training points are associated to the vector $\mathcal{Y}^{(j)} = (y_1^{(j)}, \dots, y_n^{(j)})$ of noisy observations of the objective function f_j. It is assumed that $y_i^{(j)} = f_j(\boldsymbol{x}_i) + \epsilon_i^{(j)}$, where the $\epsilon_i^{(j)}$ are independent and identically distributed Gaussian random variables having zero-mean and variance $\sigma_{\epsilon_j}^2$.

The GP construction considers that $f_j(\boldsymbol{x})$ is a realization of a zero-mean multivariate Gaussian process with covariance function C_j. We consider here the multidimensional squared exponential covariance functions defined by:

$$C_j\big(\boldsymbol{x},\boldsymbol{x}';\Theta_j\big) \doteq \theta_1 \prod_{i=1}^{d} \exp\left(\frac{-(x_i - x_i')^2}{2l_i^2}\right) + \theta_2 \tag{6}$$

where $\Theta_j = \left(\theta_1^{(j)}, \theta_2^{(j)}, l_1^{(j)}, \dots, l_d^{(j)}\right)$ is the vector of covariance hyper-parameters to be inferred from the $\mathcal{Y}^{(j)}$ observations. From the conditional rules of joint Gaussian distributions [8], the *best* prediction $\widehat{f}_j(\boldsymbol{x})$ of $f_j(\boldsymbol{x})$, *i.e.* the mean of $y^{(j)}$, and the prediction variance $\widehat{\sigma_j}^2(\boldsymbol{x})$ are given by:

$$\widehat{f}_j(\boldsymbol{x}) = \boldsymbol{k}_j^{\mathrm{T}}(\boldsymbol{x}) \left(\boldsymbol{C}_j(\Theta_j) + \sigma_{\epsilon_j}^2 \boldsymbol{I}\right)^{-1} \mathcal{Y}^{(j)} \tag{7}$$

$$\widehat{\sigma_j}^2(\boldsymbol{x}) = \kappa_j(\boldsymbol{x}) + \sigma_{\epsilon_j}^2 - \boldsymbol{k}_j^{\mathrm{T}}(\boldsymbol{x}) \left(\boldsymbol{C}_j(\Theta_j) + \sigma_{\epsilon_j}^2 \boldsymbol{I}\right)^{-1} \boldsymbol{k}_j(\boldsymbol{x}) \tag{8}$$

In (7) and (8) we have denoted $\boldsymbol{C}_j \in \mathbb{R}^{n\times n}$ the symmetric covariance matrix of the training points, $\kappa_j(\boldsymbol{x}) \doteq C_j(\boldsymbol{x},\boldsymbol{x};\Theta_j)$, $\boldsymbol{k}_j(\boldsymbol{x}) \doteq (C_j(\boldsymbol{x},\boldsymbol{x}_1;\Theta_j) \cdots C_j(\boldsymbol{x},\boldsymbol{x}_n;\Theta_j))^{\mathrm{T}}$ the covariance vector between the observations in $\mathcal{X}$ and $\boldsymbol{x}$, and $\boldsymbol{I}$ the identity matrix of $\mathbb{R}^n$. The hyper-parameters Θ_j and noise variance $\sigma_{\epsilon_j}^2$ can be determined by maximizing the log-marginal likelihood (see [8] for more details).

3.2 Merit functions under non-doable design vectors

Surrogate-based optimization methods rely on the sequential construction of statistical surrogate models, using training sets of computed objective and constraint function values, that are refined according to a prescribed infilling strategy (i.e. merit functions [10]). At each iteration of the iterative surrogate-based optimization, a new design vector $\boldsymbol{x}_{n+1}$ is thus added to $\mathcal{X}$, and finally $\boldsymbol{f}$ and $\boldsymbol{g}$ are computed. A new iteration can then start by updating surrogate models, and the iterative process is repeated until a stopping criterion is satisfied or the resources allocated to the optimization have been exhausted.

In real world applications, however, this sequential optimization procedure may stop prematurely if an objective function cannot be computed at a proposed $\boldsymbol{x}_{n+1}$. Indeed, such a situation may occur when the search space encompasses design points corresponding to a non-physical configuration or an ill-posed

problem, for example. Sacher [20] have proposed to use a classification model to learn non-doable design vector areas alongside the surrogate-based optimization and adapt the infilling strategy accordingly. In short, a probabilistic classification model is built using the union of doable and non-doable training sets. The classifier is then incorporated in the surrogate-based optimization procedure to avoid proposing new design vectors in the non-doable domain while improving the classification uncertainty if needed.

In the present work, two new design vectors are determined under the constraint to be in the doable domain and added to $\mathcal{X}$ at each new iteration of the iterative surrogate-based optimization. Specifically, the EIMH and MCPF criteria are considered (see next Sections 3.2.1 and 3.2.2) to allow respectively, the improvement of the computed Pareto front and the search of the best compromise in this Pareto Front.

3.2.1 Expected Improvement Matrix Hypervolume criterion (EIMH)

Multi-objective EI criteria have usually similar processes, where in first, an improvement function over the Pareto front is defined. In second, the expected value of the improvement function is computed by integrating it over the non-dominated region. Zhan [19] have proposed the concept of Expected Improvement Matrix (EIM) to address the usage of multi-objective EI criteria in real world applications, especially when dealing with many objective problems. This EIM concept uses a combination of $t \times m$ simple 1-D integrations to compute a cheap-to-evaluate and still efficient multi-objective EI (t is the number of non-dominated design vectors and m is the number of objectives). In [19], the scalar Expected Improvement function $EI(\boldsymbol{x})$ is expanded into a 2-D matrix EIM, in which,

$$EI_j^q(\boldsymbol{x}) \doteq \left(f_j^q - \widehat{f}_j(\boldsymbol{x})\right)\Phi\left(\frac{f_j^q - \widehat{f}_j(\boldsymbol{x})}{\widehat{\sigma_j}^2(\boldsymbol{x})}\right) + \widehat{\sigma_j}^2(\boldsymbol{x})\phi\left(\frac{f_j^q - \widehat{f}_j(\boldsymbol{x})}{\widehat{\sigma_j}^2(\boldsymbol{x})}\right) \tag{9}$$

where $j = 1, \ldots, m$ and $q = 1, \ldots, t$. The element $EI_j^q(\boldsymbol{x})$, in EIM, corresponds to the EI of the studying point $\boldsymbol{x}$ beyond the qth non-dominated front point in the jth objective. From the EIM matrix, Zhan [19] have then proposed three infilling criteria (Euclidean distance, Maximin distance and Hypervolume improvement) to aggregate the EIM into a scalar value to measure the overall improvement of the studying point compared against the Pareto front. In the present work, the Hypervolume-based EIM criterion is applied, leading to the selection of a design vector variable $\boldsymbol{x}_{EIMH}$. For more details on the EIMH criterion, interested readers are referred to [19].

3.2.2 Median Compromise of the Pareto Front (MCPF)

Solving multi-objective optimization problems leads to the search of the optimal set of solutions (i.e. Pareto front). In most real-word applications, a design vector from the Pareto set has to be selected to provide an optimal design choice. This selection is thus a compromise choice, which is usually based on the knowledge of the designer. With the aim of avoiding this designer compromise selection, the MCPF criterion is used in the present work, and is given by:

$$\boldsymbol{x}_{MCPF} \doteq \underset{\boldsymbol{x}\in\mathcal{X}_{PF}}{\arg\min}\left(\sum_{j=1}^{m} \arg\operatorname{sort}\left(\widehat{\boldsymbol{f}}_{PF_j}, \widehat{f}_j(\boldsymbol{x})\right)^2\right) \tag{10}$$

where, $\arg\mathrm{sort}(\boldsymbol{f},f) \doteq \{q \in \{1,\ldots,t\} \mid f < f_q \in \boldsymbol{f}\}$ and $\widehat{\boldsymbol{f}}_{PF_j}$ is the vector of objective function j predictions on the Pareto set $\mathcal{X}_{PF}$, which is composed of t non-dominated design vectors. As can be seen in Eq. (10), the median trade-off is selected by considering the rank, from the Pareto set, of each objective function prediction. This definition allows a design vector compromise to be determined without the need for weights or scaling of objective function.

4 Experimental measurements and optimization results

First experiments are undertaken at the Ifremer flume tank for sinusoidal pitching laws with the SHIVA platform. The measurements have been done for various advance parameter values to evaluate the performances of the cycloidal propeller over a range of operating conditions. Then the optimization procedure is carried out for λ=1.2.

4.1 Sinusoidal pitch results

All the results with sinusoidal laws are measured with the following experimental conditions: configuration of SHIVA with a diameter D=0.8 m and blade chord of c=0.35 m leading to a solidity of σ=2.625. The tank speed V is set at 0.8 m/s corresponding to a global Reynolds number $Re = \frac{VD}{\nu}$=640 000. The rotational speed Ω is then adjust to the desired λ value (see the Table 1).

λ	0.8	1	1.2	1.4	1.6	1.8	2.0	2.2	2.4
Ω (RPM)	23.87	19.09	15.92	13.64	11.94	10.61	9.55	8.68	7.96

Table 1: Corresponding table between the advance parameter λ and the rotational speed Ω.

Measurements are registered on 30 rotations of the platform after waiting that the flow is well established. Blade-control parameters are adjusted in function of the rotational speed to ensure a pitch track with a maximal error under 1 degree. Signals from the instrumentation are converted in force and projected to calculate the thrust force and main torque. These signals are then phase-averaged over the 30 periods and non-dimensionalized according equations 4. More details of the signals treatment for these experiments is providing by Fasse [2].

Global results of sinusoidal laws are given in the Figure 7. The thrust coefficient is represented by colored dotted lines with square markers whereas torque coefficient is represented by colored dashed lines with star markers. Both variables are referred with the left axis. The efficiency is represented by colored lines with circle markers and referred with the right axis.
Results reveal that depending on the value of the advance parameter, each pitch law is interesting with a maximal efficiency reached for different values of λ. This first conclusion corroborates the benefit of an adaptable pitch system to adjust the pitch to the desired operating mode. It also means that during the acceleration phase, it is preferable to start with high amplitude pitch law then decrease the pitch amplitude. However, the results for the Sinus40 law show that for λ<1, a trochoidal law is not well-suited for the epicycloidal mode. The transition between epicycloidal and trochoidal mode is complex in term of pitch law shape and requires a specific investigation that is not detailed in this paper. Furthemore, because motors of the platform have encountered some limitations in epicycloidal (explained in Section 2.2), the study presented here is focused on the trochoidal mode.
Concerning the thrust, the Sinus10 law has the higher values for all the advance parameters. It shows that for manoeuvre which requires high thrust, the pitch amplitude must be decreased, balancing a reduction

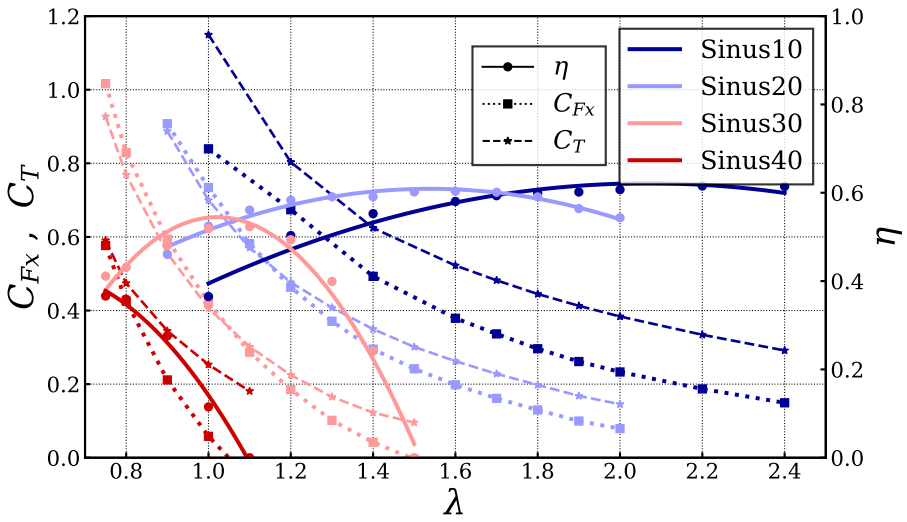

Figure 7: Global performances (Thrust and Torque coefficients at the left scale and Efficiency at the right scale) for four amplitudes of sinusoidal laws.

of the efficiency. But the efficiency hardly falls for λ close to 1 because the required torque to rotate the propeller is rising.

Sinusoidal pitch law are suited for mechanic pitch systems as periodic and symmetrical blade motion (as studied by Bose [22] and Roesler [3]). But there is no reason why the pitch law definition should be symmetrical. Indeed, the complexity of the flow through cross-flow propellers implies a strong discrepancy between upstream and downstream halves. It is why an experimental optimization is proceeded with a relevant parameterization of the pitch law (detailed previously).

4.2 Optimized pitch results

Experimental conditions for the optimization are as follows: λ=1.2, tank speed V=0.8 m/s, SHIVA rotational speed Ω=15.92 RPM. Before tackle the optimization, a sampling of 35 pitch laws is realized through the parametric space using Latin Hypercube Sampling method [23]. Then approximately 50 optimization steps have been performed during 8 hours of experiments (approximately 10 minutes by step). One step of optimization consists on:

1. Generate the pitch law with the three parameters (x_1, x_2, x_3).
2. Upload the pitch law on the SHIVA platform and start the measurement of force signals after waiting few minutes that the flow is well established.
3. After a duration corresponding to 30 rotations of SHIVA, measurements are post-treated to calculate the value of objective function (here is the mean thrust coefficient C_{F_X} and the efficiency η)
4. These new data are computed to update the two meta-models of thrust and efficiency and the Pareto Front.
5. The optimizer gives back two new triplet of parameters after computing the EIMH and the MCPF criterion to respectively search for the best improvement for both objectives and search for the best

compromise on the Pareto Front.

6. Return to the stage one.

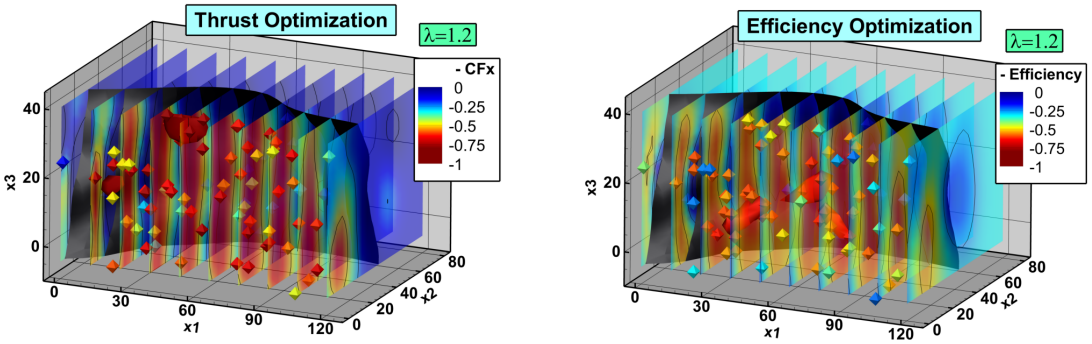

Figure 8: Meta-models for Thrust (left) and Efficiency (right) at the end of multi-objective optimization.

Figure 8 gives the two meta-models in the 3d parametric space at the end of optimization. Octahedrons are the experimental points located in function of the parameters which were used to generated the pitch law. As mentioned earlier, all experimental points are inside the front area delimited by the black 50%-probability iso-surface. Octahedrons are colored with their objective value (total thrust coefficient at the left and efficiency at the right). Slices show the meta-model inferred from experimental points and so colored in function of the objective value. Lastly, for respectively the thrust and the efficiency, the red iso-surface represents the pockets of the meta-model for which the thrust coefficient is higher than 0.75 (absolute value) and respectively higher than 0.63 for the efficiency. Because the optimizer uses a minimization procedure during the optimization, objective function are given with negative sign.
These results show that the pocket of maximal thrust is not located in the same area than this for efficiency. It proves that for λ=1.2, the blade motion which produces the maximal thrust is not this which is the best efficient. The law which maximize the thrust is generated by the triplet (48.88, 7.37, 39.19) whereas this which maximize the efficiency is given by the triplet (37.07, 17.92, 8.93). According to the value of parameter x_2, which deals with the amplitude of the law, optimization shows that the law with the best efficiency has an amplitude around 20° whereas for thrust maximizing the amplitude of the law is lower. This result confirms observations about sinusoidal laws for which Sinus20 have a better efficiency at λ=1.2 than Sinus10 but a lower thrust coefficient (see Figure 7).

These two meta-models reveal that there is a compromise between thrust maximization and hydrodynamic efficiency. The Median Compromise of the Pareto Front criterion, which is based on ranking trade-off between multiple objectives, permits to search for the best law satisfying both objectives without regarding objective values but only the rank of each objective through all measured laws. The best compromise is the law for which the sum of the rank is minimum. Thus no weighting of objectives is necessary.

Figure 9 presents the Pareto Front obtained from the experimental optimization. The little colored circles correspond to each generated laws and are plotted in function of the experimental results in thrust coefficient and efficiency pairs. Black squares correspond to a virtual front estimated by the optimizer based on the experimental results. Finally, sinusoidal results for λ=1.2 are displayed to compare performances.
As expected, there are significant performance benefits to be gained with optimized law for both objectives. The efficiency gain is around **8**% between Sinus20 and the Pareto Front ($\eta_{Sinus20}$ = 0.57

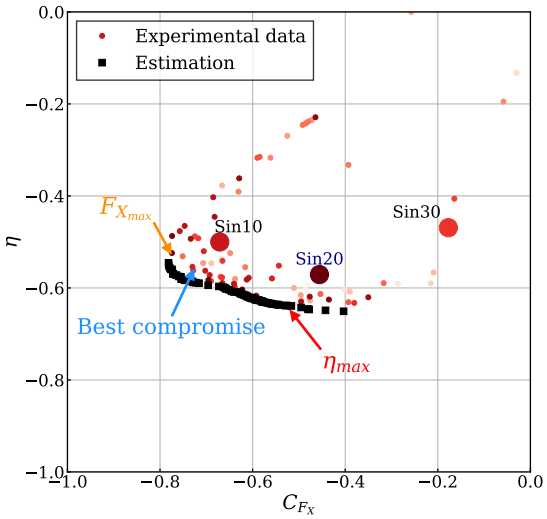

Figure 9: Pareto front obtained from experimental optimization and compared to sinusoidal pitch results.

and η_{Optim} = 0.64) while the advantage in thrust is over **11**% between Sinus10 and the Pareto Front ($CF_{X_{Sinus10}}$ = 0.67 and $CF_{X_{Optim}}$ = 0.78).

Figure 10 gives general results (pitch law φ and blade forces F_X and F_Y) for the 20-sinusoidal law (in dark blue) and three optimized laws: with the best thrust (in orange), the best efficiency (in red) and the best compromise (in light blue). The right sub-figure shows the experimental measurement of hydrodynamic forces along θ positions (each 30°). These three laws are also represented in the Figure 9 as well as the Sinus20 law.

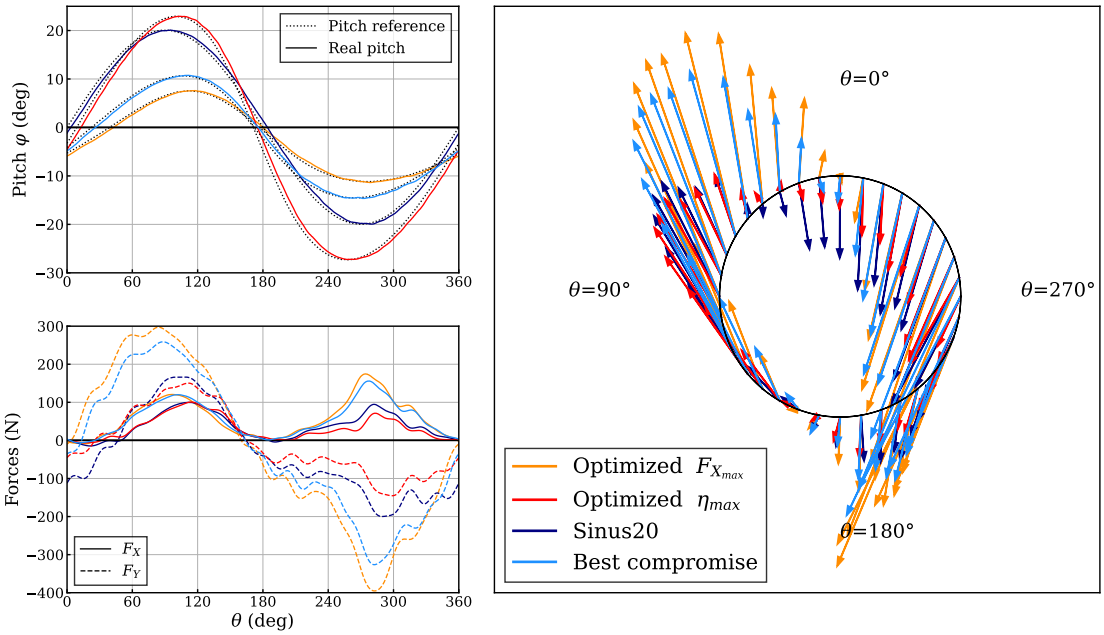

Figure 10: Detailed results of hydrodynamic forces generated by three different laws (Sinus20, Optimized law maximizing the trust $F_{X_{max}}$ and Optimized law maximizing the efficiency η_{max}) over azimuth positions.

Concerning the pitch law, optimization procedures reveal two main differences with sinusoidal laws:

- Non-zero pitch at θ=0° (dephasing effect)
- Higher pitch for downstream positions than for upstream positions (non-symmetrical effect)

The first effect is due to the x_3 parameter which forces the law to cross the φ=0-line at θ=x_3 (θ=39.19° for the thrust maximization law and θ=8.93° for the efficiency maximization law). While sinusoidal law passes through the point (θ=0,φ=0), optimized laws have slight incidence at θ=0°. This leads to a reduction of the hydrodynamic forces near θ=0° especially side force component F_Y. For these positions, thrust force is close to zero, so the reduction of side force have a favorable effect on the efficiency. Indeed, by decreasing the hydrodynamic loads at these positions the total torque required to turn the whole platform is also reducing.
The non-symmetrical effect has two different impacts regarding the optimized laws. For the $F_{X_{max}}$ law, the thrust peak in the upstream is shifted towards θ=90° (whereas the peak is reached near θ=120° for the two other laws). In the downstream half, the thrust peak is even higher than the upstream half, contrary to the η_{max} and the Sinus20 laws for which the downstream thrust is lower than in upstream. But the thrust increasing comes with a side-force inflation which induces a diminution of efficiency. For the η_{max} law, the non-symmetrical effect leads to significant decrease the side-force F_Y in the downstream half in comparison with the Sinus20 and other optimized law, while thrust force is quite similar to the Sinus20 law. And so the required torque to the main rotation is lower than the classic sinusoidal law which implies a better efficiency. Finally the law which have the best compromise between thrust and efficiency has a pitch shape located between $F_{X_{max}}$ law and η_{max} law. Concerning the thrust, this law is similar to the $F_{X_{max}}$ law in the upstream and almost for the downstream. But the significant gain is on the side-force which is clearly lower than for the $F_{X_{max}}$ law, resulting to a better efficiency.

This trade-off between efficiency and thrust can be modified into the search of the law giving the best efficiency for a given value of thrust. Indeed, for propulsion purpose, the idea is to reach a desired advance speed while overcoming the hull resistance. So knowing this hull resistance, which depends on the hull shape, dimensions and the advance speed, this procedure is very interesting for the design of vertical axis propeller.
To go further, a generalization of this optimization for different λ values ensures an optimal law for a wide range of velocities and operation modes.

5 Conclusion and Perspectives

This paper presented an experimental optimization procedure of a cycloidal propeller blade pitch laws. Indeed, for this specific type of propulsion, characterized by the rotation of blades around an axis perpendicular to the ship advance speed, the blade motion has a huge impact on the propeller performances. Traditional cycloidal propellers have a mechanical system which deals with the blade pitch rotation. These systems, represented by sinusoidal pitch law in trochoidal mode (λ >1 systems), show limitations in term of efficiency. A fully electric system, as the SHIVA platform described in this paper, can surpass the performances by managing non-symmetrical blade pitch laws.
By using a suitable parameterization of the pitch laws allowing a wide diversity of pitch motion, the multi-objective optimization is performed on experimental measurements of the SHIVA platform at the Ifremer current tank. Both thrust and efficiency maximization are chased to satisfy two different objectives. Results shows that a trade-off is necessary concerning the pitch law shape to maximize the thrust or the efficiency. A Pareto Front is thus determined between these two objectives to search for the best

compromise law. The results and the comparison with sinusoidal results show a significant improvement of both thrust and efficiency for the best compromise.
Finally, because experimental optimization takes time, the procedure have been carried out for only one λ value. As perspectives, it will be interesting to repeat this optimization for a range of λ values to compare the performances of the cycloidal propeller for many operating points. Computational Fluid Dynamic calculations using FINE/Marine commercial code (2D Unsteady Reynolds Averaged Navier-Stokes) are currently performed with the experimental facilities dimensions. The same optimisation procedure could be numerically achieved to compare the optimization results. An other perspective is to upgrade the SHIVA platform with the installation of a Artificial Intelligence to deal with the automatizing of the optimization. Indeed, here the optimization is performed step by step during long measurements. But because the platform is instrumented with embedded load sensors, it could process an automatic optimization for various experimental conditions (such as diverse tank or rotational velocities).

References

[1] M. Triantafyllou, A. Techet, F. Hover, Review of Experimental Work in Biomimetic Foils, Journal of Ocean Engineering, IEEE, 29 (3) 585–594, 2004.

[2] G. Fasse, F. Becker, F. Hauville, J.A. Astolfi, G. Germain, An experimental blade-controlled platform for the design of smart cross-flow propeller, Ocean Engineering, Elsevier, vol. 250, 110921, 2022.

[3] B.T. Roesler, M.L. Kawamura, E. Miller, M. Wilson, J. Brink-Roby, E. Clemmenson, M. Keller, B.P. Epps, Experimental performance of a novel trochoidal propeller, Journal of Ship Research, 60 (1) 48–60, 2016.

[4] M. Sacher, F. Hauville, R. Duvigneau, O. Le Maitre, N. Aubin, M. Durand, Efficient optimization procedure in non-linear fluid-structure interaction problem: Application to mainsail trimming in upwind conditions, Journal of Fluids and Structures, 69 209–231, 2017.

[5] E. Schneider, Blade Wheel, US Patent 168150, URL: https://patents.google.com/patent/US1681500, 1928.

[6] S. Abbaszadeh, S. Hoerner, T. Maître, R. Leidhold, Experimental investigation of an optimised pitch control for a vertical-axis turbine, IET Renewable Power Generation, 13 (16) 3106–3112 , 2019.

[7] T.W. Simpson, J.D. Poplinski, N.P. Koch, J.K. Allen, Metamodels for Computer-based Engineering Design: Survey and recommendations, Engineering with Computers, 17 (2) 129–150, 2001.

[8] C. Williams, C.E. Rasmussen, Gaussian processes for machine learning, MIT press Cambridge, 2 (3), 2006.

[9] J.P.C. Kleijnen, Kriging metamodeling in simulation: A review, European Journal of Operational Research, 192 (3) 707–716, 2009.

[10] V. Picheny, T. Wagner, D. Ginsbourger, A benchmark of kriging-based infill criteria for noisy optimization, Structural and Multidisciplinary Optimization, 48 (3) 607–626, 2013.

[11] D.R. Jones, M. Schonlau, W.J. Welch, Efficient Global Optimization of Expensive Black-Box Functions, Journal of Global optimization, Springer, 13 (4) 455–492, 1998.

[12] M. Sacher, F. Hauville, R. Duvigneau, O. Le Maître, N. Aubin, M. Durand, Efficient optimization procedure in non-linear fluid-structure interaction problem: Application to mainsail trimming in upwind conditions, Journal of Fluids and Structures, 69 (7) 209–231, 2017.

[13] M. Sacher, M. Durand, E. Berrini, F. Hauville, R. Duvigneau, O. Le Maître, J.A. Astolfi, Flexible hydrofoil optimization for the 35th America's Cup with constrained EGO method, Ocean Engineering, 157 62–72, 2018.

[14] M. Meliani, N. Bartoli, T. Lefebvre, M.A. Bouhlel, J. Martins, J. Morlier, Multi-fidelity efficient global optimization : Methodology and application to airfoil shape design, AIAA Aviation 2019 Forum, Dallas, 2019.

[15] J. Svenson, T.J. Santner, Multiobjective optimization of expensive black-box functions via expected maximin improvement, The Ohio State University, Columbus, 32, 2010.

[16] A.J. Keane, Statistical improvement criteria for use in multiobjective design optimization, AIAA journal, 44 (4) 879–891, 2006.

[17] C. Luo, K. Shimoyama, S. Obayashi, Kriging model based many-objective optimization with efficient calculation of expected hypervolume improvement, IEEE Congress on Evolutionary Computation (CEC), 1187–1194, 2014.

[18] A.G. Passos, M.A. Luersen, Multiobjective optimization of laminated composite parts with curvilinear fibers using Kriging-based approaches Structural and Multidisciplinary Optimization, Springer, 57 (3) 1115–1127, 2018.

[19] D. Zhan, Y. Cheng, J. Liu, Expected improvement matrix-based infill criteria for expensive multiobjective optimization, IEEE Transactions on Evolutionary Computation, 21 (6) 956–975, 2017.

[20] M. Sacher, R. Duvigneau, O. Le Maitre, M. Durand, E. Berrini, F. Hauville, J.A. Astolfi, A classification approach to efficient global optimization in presence of non-computable domains, Structural and Multidisciplinary Optimization, Springer, 58 (4) 1537–1557, 2018.

[21] K. Deb, A. Pratap, S. Agarwal, T. Meyarivan, A fast and elitist multiobjective genetic algorithm: NSGA-II, IEEE transactions on evolutionary computation, 6 (2) 182–197, 2002.

[22] N. Bose, P.SK. Lai, Experimental performance of a trochoidal propeller with high-aspect-ratio blades, Marine Technology and SNAME News, 26 (3) 192–201, 1989.

[23] M.D. Mckay, R.J. Beckman, W.J. Conover, A comparison of three methods for selecting values of input variables in the analysis of output from a computer code, Technometrics, 42 (1) 55–61, 2000.